

Kepler’s first view of O-star variability: K2 data of five O stars in Campaign 0 as a proof-of-concept for O-star asteroseismology^{*}

B. Buysschaert^{1,2,†}, C. Aerts^{2,3}, S. Bloemen³, J. Debosscher², C. Neiner¹, M. Briquet^{4,1,‡},

J. Vos², P. I. Pápics^{2,§}, R. Manick², V. Schmid^{2,¶}, H. Van Winckel², A. Tkachenko^{2,||}

¹ LESIA, Observatoire de Paris, PSL Research University, CNRS, Sorbonne Universités, UPMC Univ. Paris 06, Univ. Paris Diderot, Sorbonne Paris Cité, France

² Instituut voor Sterrenkunde, KU Leuven, Celestijnenlaan 200D, 3001 Leuven, Belgium

³ Department of Astrophysics/IMAPP, Radboud University Nijmegen, 6500 GL Nijmegen, The Netherlands

⁴ Institut d’Astrophysique et de Géophysique, Université de Liège, Quartier Agora, Allée du 6 août 19C, B-4000 Liège, Belgium

Accepted ?; Received 2015 June 17; in original form 2015 June 17

ABSTRACT

We present high-precision photometric light curves of five O-type stars observed with the refurbished *Kepler* satellite during its Campaign 0. For one of the stars, we also assembled high-resolution ground-based spectroscopy with the HERMES spectrograph attached to the 1.2-m Mercator telescope. The stars EPIC 202060097 (O9.5V) and EPIC 202060098 (O7V) exhibit monoprotic variability due to rotational modulation with an amplitude of 5.6 mmag and 9.3 mmag and a rotation period of 2.63 d and 5.03 d, respectively. EPIC 202060091 (O9V) and EPIC 202060093 (O9V:pe) reveal variability at low frequency but the cause is unclear. EPIC 202060092 (O9V:p) is discovered to be a spectroscopic binary with at least one multiperiodic β Cep-type pulsator whose detected mode frequencies occur in the range $[0.11, 6.99] \text{d}^{-1}$ and have amplitudes between 0.8 and 2.0 mmag. Its pulsation spectrum is shown to be fully compatible with the ones predicted by core-hydrogen burning O-star models. Despite the short duration of some 33 d and the limited data quality with a precision near $100 \mu\text{mag}$ of these first K2 data, the diversity of possible causes for O-star variability already revealed from campaigns of similar duration by the MOST and CoRoT satellites is confirmed with *Kepler*. We provide an overview of O-star space photometry and give arguments why future K2 monitoring during Campaigns 11 and 13 at short cadence, accompanied by time-resolved high-precision high-resolution spectroscopy opens up the possibility of in-depth O-star seismology.

Key words: Asteroseismology – Stars: massive – Stars: rotation – Stars: oscillations (including pulsations) – Techniques: photometry – Techniques: spectroscopy

1 INTRODUCTION

Recent high-precision uninterrupted high-cadence space photometry implied a revolution in the observational evaluation of stellar structure models for various types of low-mass stars, covering almost their entire evolutionary path. Many results were obtained for *sun-like stars and red giants* undergoing solar-like oscillations excited stochastically in their convective envelope, thousands of which were monitored. The interpretation of their oscillation spectrum is readily achieved by relying on existing methodology developed for helioseismology, when extended with the interpretation of gravity-dominated dipole mixed modes (e.g., Bedding et al. 2011; Mosser et al. 2012; Chaplin & Miglio 2013). Although many open questions remain on the evolutionary state of blue horizontal branch stars (e.g., Østensen et al. 2012), progress was also achieved from asteroseismology of a few subdwarf B stars and white dwarfs. These are *evolved low-mass stars*, the former of which have lost almost their entire hydrogen envelope while passing through the he-

^{*} Based on the data gathered with NASA’s Discovery mission *Kepler* and with the HERMES spectrograph, installed at the Mercator Telescope, operated on the island of La Palma by the Flemish Community, at the Spanish Observatorio del Roque de los Muchachos of the Instituto de Astrofísica de Canarias and supported by the Fund for Scientific Research of Flanders (FWO), Belgium, the Research Council of KU Leuven, Belgium, the Fonds National de la Recherche Scientifique (F.R.S.–FNRS), Belgium, the Royal Observatory of Belgium, the Observatoire de Genève, Switzerland and the Thüringer Landessternwarte Tautenburg, Germany.

[†] E-mail: bram.buysschaert@obspm.fr

[‡] F.R.S.–FNRS Postdoctoral Researcher, Belgium

[§] Postdoctoral Fellow of the Fund for Scientific Research of Flanders (FWO), Belgium

[¶] Aspirant PhD Student of the Fund for Scientific Research of Flanders (FWO), Belgium

^{||} Postdoctoral Fellow of the Fund for Scientific Research of Flanders (FWO), Belgium

lium flash in a binary configuration (e.g., Van Grootel et al. 2010; Charpinet et al. 2011). The latter are the *compact remnants of low-mass stars* that were very successfully studied from ground-based mmag-precision asteroseismology more than two decades ago (e.g., Córscico et al. 2008, and references therein) but they were hardly monitored seismically from space due to their faintness and fast oscillations of tens of seconds (Østensen et al. 2011; Bischoff-Kim & Østensen 2011; Hermes et al. 2011). The heat-driven pressure and/or gravity modes detected in hundreds of *intermediate-mass stars* are much harder to analyse and interpret theoretically than the stochastically-excited solar-like pulsators, but major progress is also underway for such objects (Kurtz et al. 2014; Saio et al. 2015; Van Reeth et al. 2015).

From the point of view of chemical evolution of our Milky Way, *supernova progenitors*, i.e., stars with masses above $\sim 9 M_{\odot}$ having an extended convective core and a radiative envelope at birth, are the objects that matter (Maeder 2009). Despite their large importance for massive star evolution theory, *O stars have hardly been monitored in high-cadence uninterrupted space photometry*. If available, such monitoring was so far restricted to mmag precision obtained by the WIRE, MOST, and Coriolis (SMEI instrument) satellites, while CoRoT observed six O stars during 34 d leading to a level of brightness variations with $\sim 100 \mu\text{mag}$ in precision. Except for the SMEI light curves, which are seven to eight months long, all of the available time series have a duration of the order of a month only.

Unfortunately, O stars were absent in the nominal *Kepler* Field-of-View (FoV), hence we do not have long-term μmag -level precision photometry of O stars at hand, preventing detailed asteroseismic calibrations of massive star models as it was achieved for the less massive B stars (e.g. Aerts 2015, for a summary). Similarly to the O stars, B stars have an extensive convective core but they do not exhibit a strong radiation-driven wind. The two B stars that were seismically modelled based upon period spacings of their high-order dipole gravity-mode oscillations are ultra-slow rotators ($v \sin i < 10 \text{ km s}^{-1}$). Their modelling required the inclusion of extra diffusive mixing, in addition to core overshooting, to bring the theoretical models in agreement with the μmag -precision seismic data of duration five months (for the B3V star HD 50230, Degroote et al. 2010) and four years (for the B8V star KIC 10526294, Moravveji et al. 2015). It would be highly beneficial to perform similar seismic inference studies for O-type stars, whose theoretical models are the most uncertain of all the mass ranges, while they are mainly responsible for the global chemical enrichment of the Milky Way.

Two rapidly rotating O stars were monitored by the MOST satellite. It concerns ξPer (O7III_{nf}) with $v \sin i \approx 200 \text{ km s}^{-1}$ revealing variability due to rotational modulation with a rotation period of 4.18 d, in the absence of oscillations (Ramiaramantsoa et al. 2014) and ζOph (O9.5V_{nn}, $v \sin i \approx 400 \text{ km s}^{-1}$) whose WIRE, MOST, SMEI photometry led to the detection of multiperiodic variability due to oscillations with frequencies in the range $[1, 10] \text{ d}^{-1}$ and amplitudes up to $\approx 10 \text{ mmag}$. These modes turn out to be variable on a time scale of some 100 d (Howarth et al. 2014). The rapid rotator ζPup was monitored by SMEI during several long-term runs, but these data revealed only two dominant frequencies, whose cause and identification remain unclear; they might be connected with non-adiabatic gravity modes (Howarth & Stevens 2014). The variability derived from the space photometry of these three rapid rotators is in line with assessments from their high-precision time-resolved line-profile variability. It is also in agreement with high-precision time-resolved spec-

troscopy of the rapidly rotating O9Vp star HD 93521, whose multiperiodicity has a yet unclear origin (e.g., Fullerton, Gies, & Bolton 1996; Rauw et al. 2008, $v \sin i \approx 400 \text{ km s}^{-1}$). Seismic modelling of rapidly rotating O stars was not achieved so far.

One of the CoRoT short runs (SRa02) was devoted to the monitoring of six O-type stars during 34 d in the asteroseismology CCD of the mission, having a cadence of 32 s (Auvergne et al. 2009). Among these six stars were two binaries. Plaskett’s star (HD 47129) is a high-mass interacting binary (O7.5I+O6II) with a magnetic secondary (Grunhut et al. 2013). Its CoRoT light curve revealed hints of gravity-mode oscillations with frequencies near $\sim 0.8 \text{ d}^{-1}$ and harmonics, as well as rotational modulation with multiples of the orbital period of 14.39625 d (Linder et al. 2008) — see Mahy et al. (2011) for a discussion. A seismic interpretation was not possible for this complex system. The eccentric ($e = 0.59 \pm 0.02$) long-orbit ($P_{\text{orbit}} = 829 \pm 4 \text{ d}$) binary HD 46149 revealed a primary with stochastic pressure-mode oscillations with frequencies in the range 3.0 to 7.2 d^{-1} . These correspond to a regular frequency pattern of separation 0.48 d^{-1} . Unfortunately, these p modes did not lead to an unambiguous interpretation in terms of seismic models (Degroote et al. 2010). Further, the “red noise” power excess found by Blomme et al. (2011) in the CoRoT amplitude spectra of the three moderately rotating O stars HD 46150 (O5.5f, $v \sin i \approx 100 \text{ km s}^{-1}$), HD 46223 (O5f, $v \sin i \approx 100 \text{ km s}^{-1}$), and HD 46966 (O8.5V, $v \sin i \approx 50 \text{ km s}^{-1}$) were recently interpreted in terms of convectively-driven internal gravity waves (Aerts & Rogers 2015).

The only seismic inference was achieved for the O9V star HD 46202, which revealed βCep -type pressure-mode oscillations with frequencies in the range from 0.5 to 4.9 d^{-1} (Briquet et al. 2011). Seismic modelling of this star led to a mass $M = 24.1 \pm 0.8 M_{\odot}$, an age of $4.3 \pm 0.5 \text{ Myr}$, and a core overshooting parameter of 0.10 ± 0.05 expressed in units of the local pressure scale height and using a step-function formulation.

To remedy the lack of seismic calibration of massive star models, we defined a K2 (Howell et al. 2014) observing programme of O-type stars with the aim to monitor a sample of such objects at μmag precision during 3-month runs. The present work reports on the first results of this programme and offers a proof-of-concept of K2’s capabilities for future O-star asteroseismology.

2 EXTRACTION OF THE LIGHT CURVES

We proposed the five O-type stars listed in Table 1 for photometric monitoring with K2 in Campaign 0. We developed a photometric reduction method that accounts for the spacecraft (re)pointing and the non-uniform pixel response of the K2 CCDs, starting from the pixel frames in the MAST archive (release of 7 Nov. 2014). The time series of Campaign 0 contain two large gaps related to safety events of the spacecraft. We only used data after the largest safety event, i.e., after the *Kepler* Barycentric Julian Day 1939.1, providing us with photometric measurements covering 33.038 d. These data have a frequency resolution corresponding to the Rayleigh limit of $1/33.038 \text{ d} = 0.0302 \text{ d}^{-1}$ ($0.35 \mu\text{Hz}$), which represents an upper limit for the frequency uncertainty of any periodic signal in the data (Aerts et al. 2010, Chapter 5). Further, we ignored all measurements taken during a thruster firing or a repointing event of the spacecraft.

With the aim to exclude as much as possible instrumental effects in the light curves, we first defined an optimal constant mask *customized to each of the five targets from visual inspection*, such

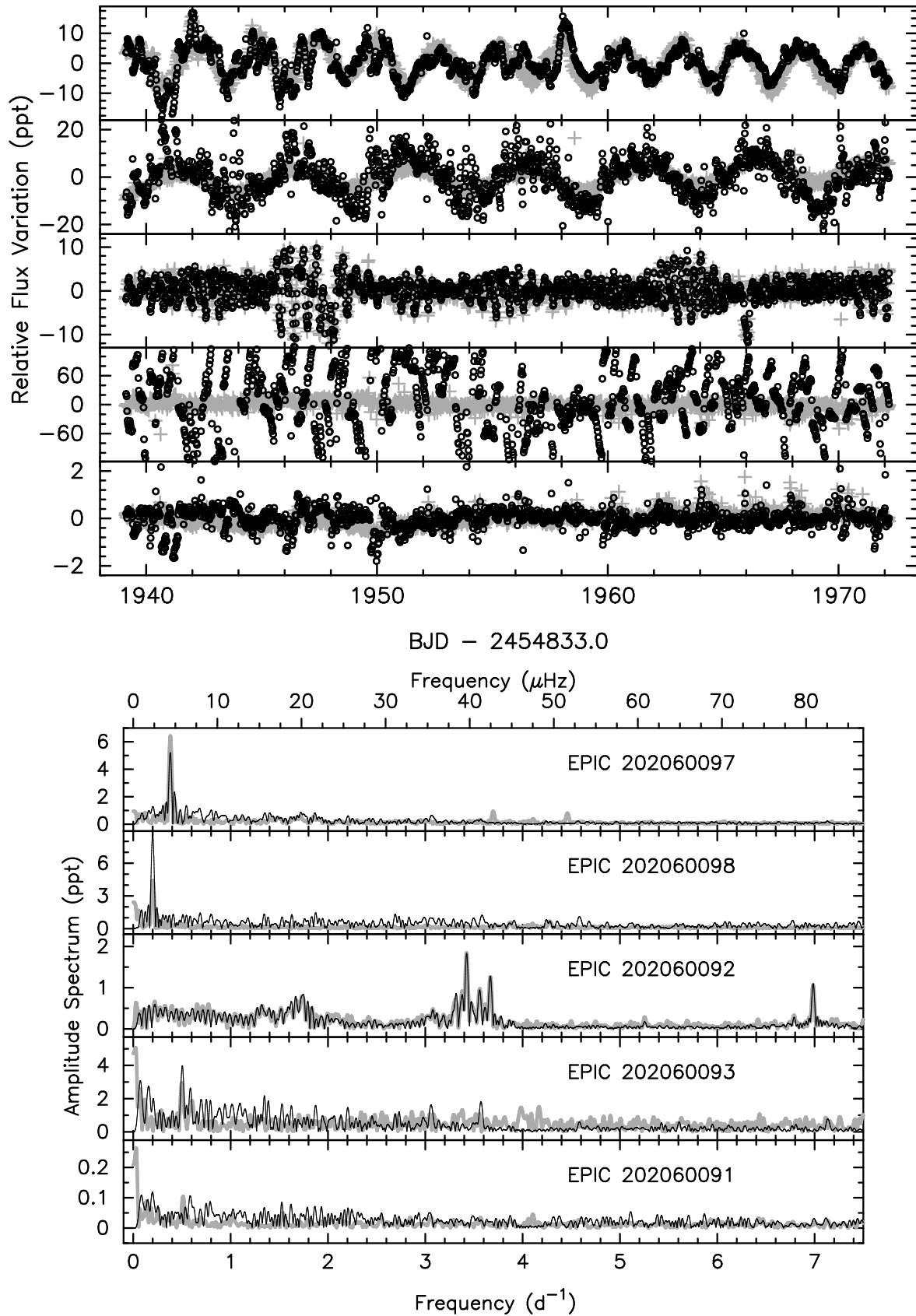


Figure 1. K2 light curves (top) and their amplitude spectra (bottom) of the five monitored O stars. The black circles and thin black lines are derived from our reduction of the raw pixel data, while the grey crosses and thick grey lines are the Vanderburg (2014) light curves.

Table 1. The five O stars observed in Campaign 0 of K2, with some information from the online SIMBAD database and the EPIC catalogue. The dominant frequency in the K2 data is listed, along with its amplitude.

EPIC ID	Other ID	RA (J2000)	DEC (J2000)	V (mag)	SpT	Frequency (d ⁻¹)	Amplitude (ppt)
202060091	HD 44597	06 23 28.538	+20 23 31.63	9.05	O9V	—	—
202060092	HD 256035	06 22 58.243	+22 51 46.15	9.21	O9V:p	3.4248	1.827
202060093	HD 255055	06 19 41.647	+23 17 20.22	9.40	O9V:p(e)	—	—
202060097	Cl* NGC 2175 H 98	06 08 31.999	+20 39 24.01	13.7	O9.5V	0.3801	5.209
202060098	2MASS J06245986+2649194	06 24 59.870	+26 49 19.42	15.11	O7V	0.1988	8.594

that blending with nearby targets is avoided as much as possible. We show these masks in the left panels of Figs A1 to A5. The counts for each pixel in these masks were summed up to provide the time series of the raw photometric measurements. To account for the varying background during the measurements, we used iterative sigma clipping. All pixels of the frame at a given time step were deselected when their signal was larger than 1.2 times the median signal of the frame. This procedure was iterated until we found a stable median for that time step and no further deselection was needed. The achieved median was then taken to be the background signal in a given pixel in the frame. We subtracted this background level from the raw light curve, accounting for the considered number of pixels in the mask.

Outliers were identified and removed by self-flat-fielding through spline fitting, along with further detrending of the photometry by third-order polynomial fitting, in an iterative scheme. In each step, the photometry was divided by the polynomial fit, which allowed us to work with relative brightness units instead of electrons per second. Five iteration steps turned out to be sufficient.

This raw light curve was then used as a starting point to account for the instrumental effects caused by K2’s attitude control system, which involves a roll manoeuvre every six hours. Due to that, we had to redetermine the position of the star on the CCD and connect it to the instrumental brightness variations that occurred at that position. In order to derive an appropriate relation for the correction factor versus star position, we determined the position of the star on the CCD by fitting a 2D Gaussian function to the photometry, representing the point-spread-function. Following Vanderburg & Johnson (2014), we rotated that 2D position according to its largest eigenvalue and fitted a fifth-order polynomial, allowing us to define an arclength connected with the instrumental brightness for each time step. We then assumed that all the power in the Fourier transform of the time series of the measured brightness centred at 4.08 d⁻¹ and its higher harmonics at 8.16, 12.24, 16.32, and 20.40 d⁻¹ had instrumental origin. A bandpass filter in the Fourier domain was constructed using the bands $j \times 4.08 \text{ d}^{-1} \pm 5 f_{\text{res}}$, with f_{res} the Rayleigh limit and $j = 1, \dots, 5$. All the power in these bands was assumed to be due to instrumental effects, while all power outside these bands was considered as stellar signal. The inverse Fourier transform then allowed to connect the instrumental brightness variations to the position of the star on the CCD. This method worked well for four of the five stars, EPIC 202060093 suffering from a too small onboard mask and saturation of many pixels leading to leakage outside of the frame. The light curves are shown with black circles in the upper panel of Fig. 1. These flux variations are expressed in parts-per-thousand (ppt).¹

In order to compare our reduction scheme for the individual

stars and its effectiveness, we also used the reduced light curves as made available by Vanderburg (2014), release date: 10 April 2015.² This is an updated reduction based on their self-flatfielding approach combined with high-pass filtering, designed from the viewpoint of optimal exoplanet hunting, as previously developed by Vanderburg & Johnson (2014) to which we refer for details. While our mask determination and noise treatment was done manually and tuned to each star individually and locally, Vanderburg (2014) used a semi-automated mask determination and made use of the instrumental effects of thousands of stars. Our method is tuned to get the optimal signal, while their method is focused on reducing the global noise as much as possible. The masks used by Vanderburg are shown in the right panels of Figs A1 to A5.

Despite the quite different masking, the two independent reduction methods give consistent results in terms of *frequencies*, the major difference occurring in the lowest frequency regime of the Fourier transform. This is similar to the difference already encountered for light curves of the nominal *Kepler* mission when reduced globally from the viewpoint of optimal planet hunting versus individually and tuned towards optimal asteroseismic applications. For the latter, it is typically advantageous to consider more pixels than done in the standard exoplanet pipeline, because the aim is to gather as much signal as possible for a whole range of frequencies, given the multiperiodic character of the variability. For exoplanet hunting, however, one aims to find singly periodic low-amplitude signal and therefore avoids too noisy pixels. Masking for asteroseismology as we have done here avoids complicated detrending and filters out long-term instrumental frequencies more easily, as illustrated and discussed in Tkachenko et al. (2013), but is not optimal in terms of global noise properties.

A comparison between the light curves resulting from the two independent reduction methods for the five O stars considered here is given in Fig. 1. In general, the agreement is good, except for EPIC 202060098 and EPIC 202060093. For the former star, the dominant frequency is fully consistent but its amplitude differs in value, due to the different shape and position of the chosen masks in the two methods. With our mask, we have avoided the additional bright target contributing to the overall light curve. This explains the higher amplitude compared to the “Vanderburg” light curve, while the latter leads to less power at low frequencies (cf. bottom panel of Fig. 1). For EPIC 202060093, both light curves suffer from the saturation and leakage across the CCD, but again the frequency amplitude is higher when derived from our light curve. In the rest of the paper, we used our reduced light curves to derive the frequencies and amplitudes of the five target stars, after having verified that all the listed frequencies are consistently recovered from those two versions.

¹ The conversion factor between brightness variations expressed in mmag and flux variations expressed in ppt amounts to $2.5 \log_{10} e = 1.0857$

² <https://www.cfa.harvard.edu/~avanderb/>

Table 2. The frequencies and amplitudes of EPIC 202060092 determined from Fourier analysis followed by non-linear least-squares fitting. The computation of the errors is explained in the text. The signal-to-noise ratio (SNR) was computed as the amplitude divided by the noise level of the residual light curve averaged over $[0, 10] \text{ d}^{-1}$.

ID	Frequency (d^{-1})	Amplitude (ppt)	SNR	Remark
f_1	3.4243 ± 0.0054	1.827 ± 0.079	16.9	
f_2	3.6663 ± 0.0066	1.352 ± 0.084	12.5	
f_3	6.9853 ± 0.0088	1.091 ± 0.104	10.1	
f_4	3.3173 ± 0.0113	0.938 ± 0.103	8.7	
f_5	3.5583 ± 0.0089	0.998 ± 0.105	9.2	
f_6	1.7453 ± 0.0092	0.941 ± 0.083	8.7	$f_3/4$
f_7	1.6693 ± 0.0085	0.953 ± 0.106	8.8	$f_4/2$
f_8	1.7193 ± 0.0091	0.784 ± 0.106	7.3	$f_1/2$
f_9	3.4863 ± 0.0113	0.646 ± 0.096	6.0	$f_3/2$
f_{10}	0.2223 ± 0.0113	0.705 ± 0.100	6.5	$2f_{12}$
f_{11}	0.3313 ± 0.0125	0.585 ± 0.104	5.4	$3f_{12}$
f_{12}	0.1123 ± 0.0129	0.566 ± 0.074	5.2	$f_1 - f_4 = f_2 - f_5$
f_{13}	1.3223 ± 0.0134	0.535 ± 0.095	5.0	

3 FREQUENCY ANALYSIS OF K2 DATA

We computed the Lomb-Scargle periodograms of the two versions of the light curves. These are shown in the lower panel of Fig. 1. The thin black lines are for our reduced light curves while the thick grey lines are for the Vanderburg (2014) light curves.

For the stars EPIC 202060097 and 202060098, we find one isolated significant frequency corresponding to a period of 2.631 d and 5.030 d, respectively (Table 1). We interpret their variability as due to rotational modulation.

The cause of the variability of EPIC 202060091 and 202060093 is less clear. Despite the limitations of the masks for EPIC 202060093 (Fig. A3), its frequency spectrum is similar to the one of EPIC 202060091, but there is a factor more than ten difference in the level of variability. None of these two stars shows clear periodic variability with isolated frequencies. Nevertheless, they display several low-frequency peaks that stand out of the noise level without being formally significant. This is somewhat similar to the frequency spectra of three O stars observed with the CoRoT satellite, revealing red noise power excess at low frequency that was recently interpreted in terms of convectively driven internal gravity waves (Aerts & Rogers 2015). However, we currently consider this interpretation as speculative.

EPIC 202060092 turns out to be a multiperiodic pulsator compatible with heat-driven oscillation modes, similar to HD 46202 (Briquet et al. 2011). We performed iterative prewhitening and find 13 significant frequencies when we adopt the conservative criterion of considering a frequency to be significant when its amplitude reaches above five times the noise level in the residual light curve averaged over the frequency range $[0, 10] \text{ d}^{-1}$. The frequencies and amplitudes along with their errors are listed in Table 2 while the fit to the light curve based on those 13 frequencies is shown in Fig. 2. For the computation of the frequency and amplitude errors, we took into account that the formal errors resulting from a non-linear least squares fit are only in agreement with those obtained in the Fourier domain in the case of uncorrelated data with white noise and with sufficiently high frequency resolution (e.g., Aerts et al. 2010, Chapter 5). Here, we encounter two complications: the data have only a short time base of some 33 d, leading to a limited resolving power of $1.5/33.038 \text{ d} = 0.04541 \text{ d}^{-1}$ (Loumos & Deeming 1978). Further, as is usually the case for highly sampled space photometry, the

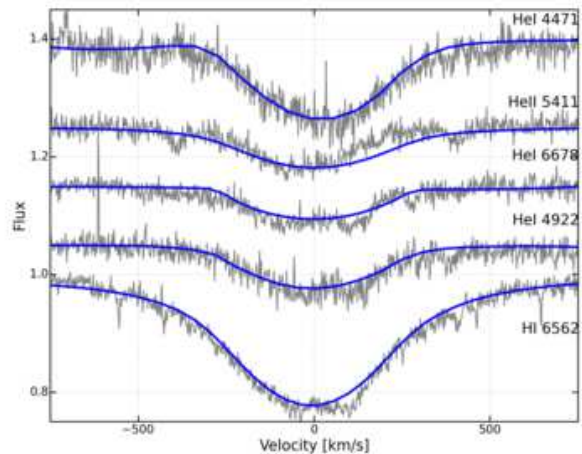


Figure 3. Selected H and He lines in the highest SNR HERMES spectrum of EPIC 202060092. The blue line is the prediction for a NLTE atmosphere model with parameters listed in the text.

data may be correlated. This requires incorporation of a correction factor in the error estimates of the frequencies and their amplitudes (Schwarzenberg-Czerny 2003). Following Degroote et al. (2009), we computed this correction factor to be 2.51 and obtained the error estimates listed in Table 2. The fit shown in Fig. 2 is generally good, but not perfect. This is due to there being additional frequencies whose amplitudes are between 3 and 5 times the noise level. Due to the limited frequency resolution, we are unable to pinpoint their value with respect to the frequencies already listed in Table 2 and this explains why a level of unresolved beating still occurs in some parts of the light curve (bottom panel of Fig. 2).

4 FOLLOW-UP STUDY OF EPIC 202060092

The nature of the frequencies f_6 to f_{13} listed in Table 2 is unclear. Given the limited frequency precision, they could either be identified as sub-multiples or combinations based on f_1 to f_5 , or be due to independent g modes occurring in the densely-packed gravity-mode frequency regime, or both. The interpretation of all the detected frequencies in terms of identification of their degree ℓ , radial order n , and azimuthal order m requires additional observational information, such as the rotational frequency of the star. We also note that the light curve of EPIC 202060092 shows a marked dip near day 1966 and remarkable beating from days 1946 to 1948 and to a lesser extent also from days 1963 to 1965 (Fig. 2, where the listed and shown dates are with respect to *Kepler* Barycentric Julian Data, indicated here as BJD 2454833.0). With the aim to test if the dips could be connected with binarity and to derive the projected rotation velocity of the pulsator, we gathered spectroscopic measurements.

4.1 EPIC 202060092 is a spectroscopic binary

The 1.2-m Mercator telescope is dedicated to the long-term monitoring of variable stars, including heat-driven pulsators (e.g., De Cat et al. 2007; Cuypers et al. 2009) and evolved low-mass stars (e.g., Van Winckel et al. 2009). A large fraction of the telescope time in the recent years has been used for the spectroscopic

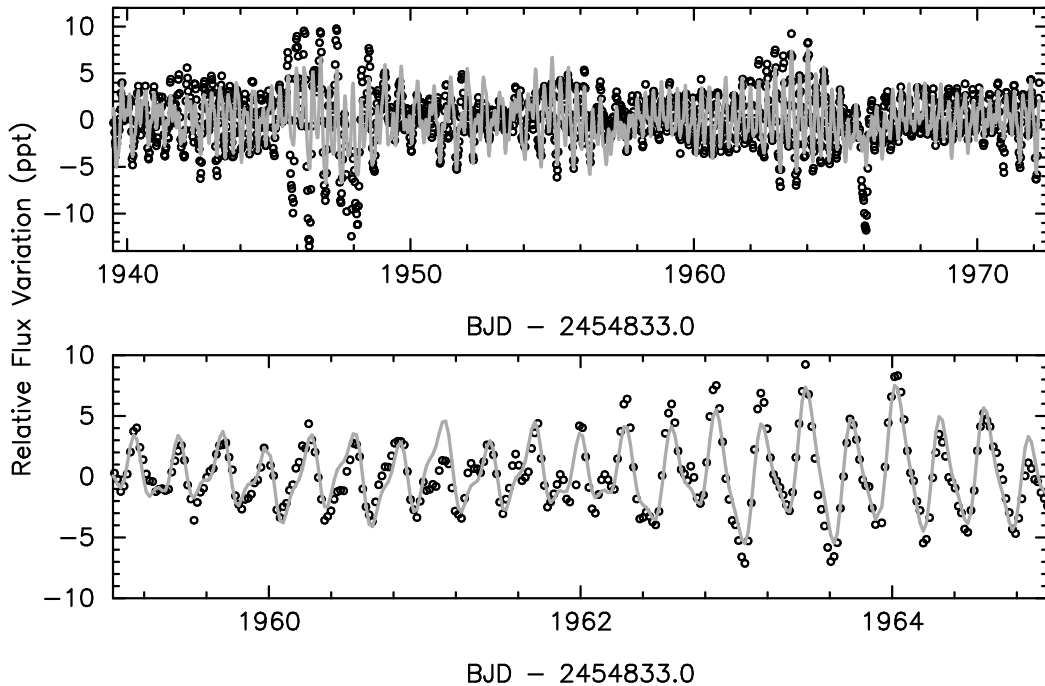


Figure 2. Fit (grey line) to the K2 light curve of EPIC 202060092 (black circles repeated from the central panel of Fig. 1) based on the 13 frequencies listed in Table 2.

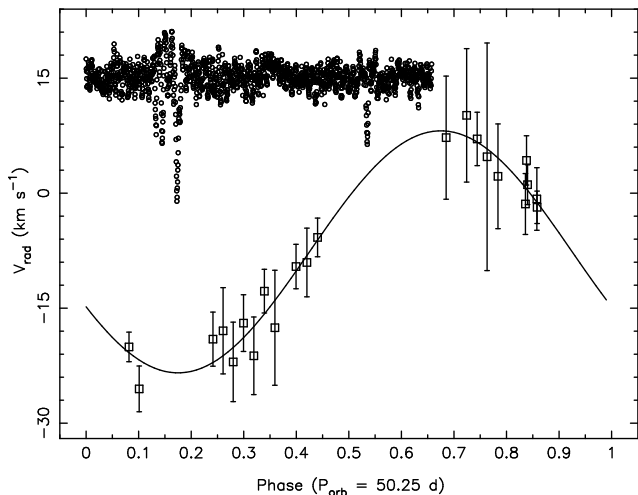


Figure 4. Phased radial velocity measurements of EPIC 202060092 deduced from its Balmer lines. The residual K2 light curve after prewhitening the fit in Fig. 2 is indicated in the top part in ppt according to the same phase and shifted up with value 15 for visibility reasons.

monitoring of bright *Kepler* targets (e.g., Lehmann et al. 2011; Tkachenko et al. 2012; Beck et al. 2014; Niemczura et al. 2015; Van Reeth et al. 2015). In view of its photometric behaviour and of recent theoretical predictions that more than 70% of all O-type stars occur in binaries (Sana et al. 2012), we added EPIC 202060092 to the observing programme for measurements with the HERMES spectrograph (Raskin et al. 2011).

A total of 22 high-resolution (HRF mode, resolution of 85 000) spectra were taken so far, with integration times between 600 s and 1800 s between November 2014 and March 2015. The signal-to-noise ratio (SNR) per exposure ranged from 30 to 60. The

raw exposures were treated with the HERMES pipeline, including cosmic-hit removal, merging of orders, and barycentric correction. Subsequently, all spectra were rectified following the method outlined in Pápics et al. (2013).

Comparison with rotationally broadened synthetic spectra derived from plane-parallel NLTE O-star atmosphere models (Lanz & Hubeny 2003, OSTAR2002 grid) led to the estimates $T_{\text{eff}} \approx 35\,000\text{ K}$, $\log g \approx 4.5\text{ dex}$, $v \sin i \approx 270\text{ km s}^{-1}$ for solar metallicity and a fixed microturbulent velocity of 10 km s^{-1} . The agreement between the theoretical line spectrum and the measured profiles for the highest SNR spectrum is illustrated in Fig. 3 for a few selected lines. Despite the modest SNR, it can be seen that structure occurs in some of the observed He lines. This may be connected to the pulsations but higher SNR is needed to firmly establish this.

Given the scarcity of spectral lines due to the large broadening and limited SNR, we estimated the radial velocity values from fits to the detected H and He lines. The outcome is very similar for the $H\alpha$, $H\beta$, $H\gamma$, and $H\epsilon$ lines, so we averaged their radial velocity estimates and computed the standard deviation as a proxy for the errors. We detect radial velocity variations with a peak-to-peak value around 30 km s^{-1} . Given the low amplitude of the photometric variations (cf. Table 2) we do not assign these radial-velocity variations to pulsations, but rather interpret them in terms of binarity. Globally, the velocities from the Balmer lines are consistent with those based on the dominant He lines, such as HeI 4922Å, HeI 5875Å, HeI 6678Å, HeII 4541Å, and HeII 5411Å, but for some of those we encounter too large uncertainties to achieve conclusive values, as already illustrated by Fig. 3. This might point towards a contribution of more than one star to some of these lines, but this needs further study from new spectra with higher SNR.

Our current spectroscopy does not allow to deduce a high-precision orbital solution yet. Nevertheless, we clearly establish spectroscopic binarity and find a rough preliminary period estimate

of $P_{\text{orb}} \sim 50$ d from the Balmer lines. These data were folded with the most likely period in Fig. 4, where we also show the phased residual K2 light curve after prewhitening the 13 frequencies listed in Table 2 (i.e., the black circles minus the grey line in Fig. 2). We conclude that, with the current estimate of the orbital period of the binary, we cannot associate all the dips in the K2 photometry with eclipses and rather ascribe them to unresolved beating of pulsation modes, except perhaps the dip near day 1966. Large beating patterns as the ones seen near days 1946, 1955, and 1964 (Fig. 2) have indeed been detected before in multiperiodic massive pulsators, both in high-cadence ground-based (e.g. Handler et al. 2004, 2006) and space photometry (e.g., Pápics et al. 2012). With the long-cadence sampling at 29 min, the unresolved nature of the light curve is not so surprising, because the fastest pulsation mode is sampled only seven times per cycle. While such sampling works fine for the analysis and interpretation of long-duration light curves of months to years, there is a limitation to resolve beating patterns for a data set of only 33 d. The beating between frequencies f_1 and f_4 , as well as the one between f_2 and f_5 , occurs with a period of 9.1 d and the beating phenomena we measure are separated by roughly this value, occurring near days 1946, 1955, and 1964 (top panel of Fig. 2). The nature of the isolated dip in the light curve at day 1966 remains unclear. That decrease in brightness is not accompanied by local increases as one would expect from multiperiodic beating among linear pulsation modes and could therefore still be caused by binarity. Indeed, according to Fig. 4, the dip occurs near orbital phase ~ 0.5 and, given the large uncertainty on the current estimate of the orbital period, could be caused by an eclipse. Unfortunately, there are no HIPPARCOS DATA data available to add to the K2 photometry for this star.

4.2 First modelling attempts

The five dominant frequencies listed in Table 2 have values typical of pressure modes in an O9 main-sequence star as already found for HD 46149 and HD 46202 by Degroote et al. (2010) and Briquet et al. (2011), respectively. Part of the theoretical radial and zonal dipole or quadrupole p mode spectrum for O-type stars is shown in Fig. 5 for a mass of $35 M_{\odot}$ (left panel) and $30 M_{\odot}$ (right panel). This figure was constructed from the grid of stellar and pulsational models described in Degroote et al. (2010), whose input physics is discussed in Briquet et al. (2011), to which we refer for details. The two stellar models whose zonal p modes are shown in Fig. 5 have an initial hydrogen fraction of $X_c = 0.715$ and a step-function core overshoot parameter of $\alpha_{\text{ov}} = 0.2$, expressed in units of the local pressure scale height. As we have shown in the previous Section, EPIC 202060092 is situated between the two vertical dashed lines. These correspond to ages of 3.53 and 3.51 Myr (hotter temperature limit) and 4.39 and 4.86 Myr (coolest temperature limit), for $35 M_{\odot}$ and $30 M_{\odot}$, respectively.

Even though relatively large uncertainties occur for the atmospheric parameters of the star, the measurement of $v \sin i$ is fairly robust. It immediately excludes $f_{12} = 0.1123 \text{ d}^{-1}$ to be the rotational frequency. Indeed, the models with $35 M_{\odot}$ and $30 M_{\odot}$ whose low-degree p modes were shown in Fig. 5 have radii of $15 R_{\odot}$ and $12.5 R_{\odot}$, respectively, for the measured T_{eff} . We find lower limits for the rotational splitting within p mode multiplets of roughly 0.36 d^{-1} and 0.43 d^{-1} for $35 M_{\odot}$ and $30 M_{\odot}$, respectively.

Even though the white-light CoRoT photometry of HD 46202 by itself did not lead to mode identification in the absence of multiplets in the frequency spectrum, the same situation as we have here for EPIC 202060092, Briquet et al. (2011) managed to perform for-

ward seismic modelling from frequency matching and pinpointed the four free parameters ($M, X, Z, \alpha_{\text{ov}}$) of HD 46202 with high precision, for the input physics that went into their dense grid of theoretical models. Their frequency precision was much higher, typically between 10^{-4} and 10^{-3} d^{-1} , than what we can deduce from the current long-cadence K2 data. This major accomplishment for HD 46202 was owed to the CoRoT sampling rate of 32 s, which delivered a light curve of more than 80 000 data points rather than only 1 600 for EPIC 202060092 from K2. Despite similar duration of the monitoring, this implies a factor $\sim \sqrt{50}$ better frequency precision. Moreover, their study was based on twice as many spectra of a single star of one magnitude brighter than EPIC 202060092, implying a co-added averaged spectrum of SNR above 500. Finally, the ten times lower $v \sin i = 25 \pm 7 \text{ km s}^{-1}$ of HD 46202 compared to EPIC 202060092 also implied modest rotational splitting values such that forward modelling assuming zonal modes made sense.

For the case of EPIC 202060092, which has a similar oscillation spectrum and hence the same potential, we encounter the limitations of the poor frequency precision and of not knowing the azimuthal order m of the dominant modes because the fast rotation introduces frequency shifts of at least 0.3 d^{-1} when $m \neq 0$. It can be seen from Fig. 5 that, even for only two masses and one set of values (X, Z, α_{ov}), several of these models fulfill the requirements of the five measured frequencies, keeping in mind that large yet unknown frequency shifts due to rotational splitting must be allowed for. A similar situation of unknown rotational shifts was encountered in the NGC 884 cluster modelling by Saesen et al. (2013), but in that study some seismic constraints could still be achieved thanks to the demand of an equal age and metallicity of the stars in the cluster.

With the present K2 photometry and HERMES spectroscopy, forward seismic modelling is not yet possible for EPIC 202060092. We do note that even the identification of (ℓ, m) of just one of its modes would break most of the degeneracy in the seismic grid. As an example, identification of f_4 as a radial mode would imply it is the fundamental, while f_3 is then the third (for $35 M_{\odot}$, left panel of Fig. 5) or fourth (for $30 M_{\odot}$, right panel of Fig. 5) radial overtone. At present, however, such inference remains speculative. Nevertheless, the models imply that, if f_1 to f_5 are due to low-degree low-order modes, then the mass of the star cannot be far below $30 M_{\odot}$.

Firm conclusions on the properties of the orbit of EPIC 202060092 and on the nature of its companion require additional and long-term time-resolved high SNR spectroscopy. Given its potential for future seismic modelling, we plan to acquire such data with the aim to pinpoint the orbit and characterise the two components with high precision, as well as to detect and identify the dominant oscillation mode(s). This will require spectral disentangling and the application of sophisticated mode identification methodology (e.g., Tkachenko et al. 2014, for an example of another potentially interesting pulsating massive binary).

5 STATE OF AFFAIRS OF HIGH-PRECISION O-STAR SPACE PHOTOMETRY

The five O-type stars monitored by K2 so far confirm earlier findings based on high-precision uninterrupted space photometry, i.e., the diversity of the variable character of these stars is large. Table 3 provides an overview of all fourteen O-type stars that have been monitored with SMEI, MOST, CoRoT, and K2 and their dominant cause of the photometric variability. For several of the stars, various causes of variability act simultaneously. The secondary of the

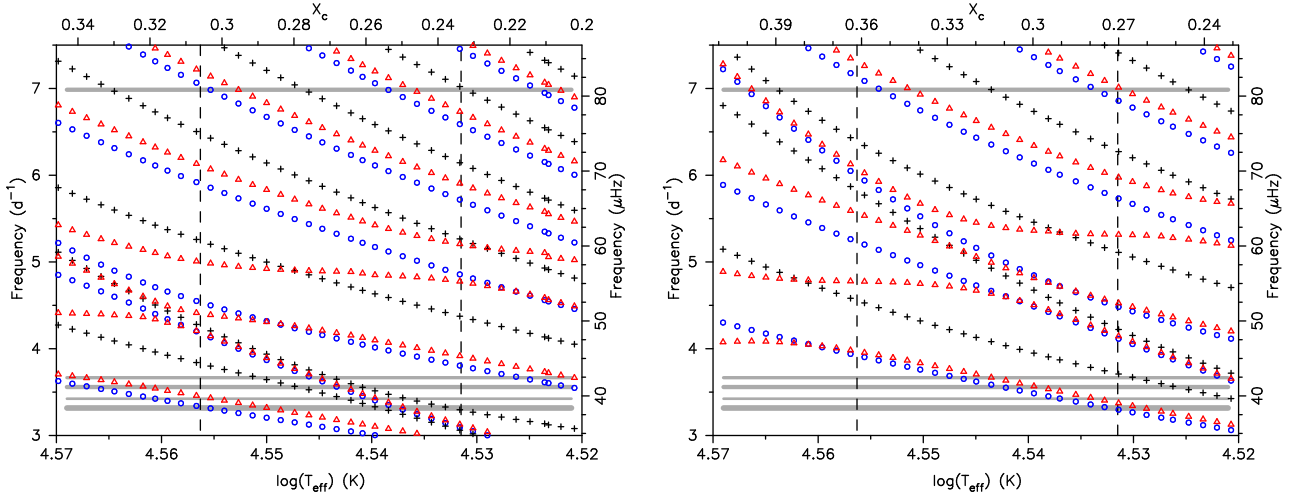


Figure 5. Adiabatic pulsation frequencies of radial (blue circles), dipole (black crosses), and quadrupole (red triangles) zonal modes for a stellar model with $M = 35 M_{\odot}$ (left) and with $M = 30 M_{\odot}$ (right). EPIC 202060092 is situated in between the two vertical dashed lines, which indicate the spectroscopic 1σ -range of the measured T_{eff} . The top x -axes indicate the central hydrogen fraction, where the value at birth was $X_c = 0.715$. The horizontal grey lines indicate the five dominant independent frequencies, where the line thickness represents the frequency precision.

Table 3. Overview of O-star variability deduced from high-cadence high-precision space photometry with the dominant causes of the variability listed, where IGW stands for “Internal Gravity Waves” (e.g. Rogers et al. 2013). The duration of the longest uninterrupted light curve is listed.

HD or EPIC	V mag	SpT	Data Source	Duration of LC (d)	$v \sin i$ km s $^{-1}$	Variability Cause(s)	Reference to Space Photometry
HD 46223	7.28	O4V(f)	CoRoT	34.3	100	IGW	Blomme et al. (2011)
HD 66811	2.24	O4I(n)fp	SMEI	236	400	non-adiabatic g^- mode?	Howarth & Stevens (2014)
HD 46150	6.73	O5V(f)	CoRoT	34.3	80	IGW	Blomme et al. (2011)
HD 24912	4.06	O7III _{nf}	MOST	30.0	200	Rotational Modulation	Ramiaramanantsoa et al. (2014)
EPIC 202060098	15.1	O7V	K2	33.1	?	Rotational Modulation	this work
HD 46966	6.87	O8V	CoRoT	34.3	50	IGW	Blomme et al. (2011)
HD 47129	6.06	O8 III/I+O7.5III	CoRoT	34.3	75 & 300	Binarity, Rotation Magnetic secondary	Mahy et al. (2011)
HD 46149	7.61	O8.5V((f))+B?	CoRoT	34.3	30 & ?	Rotational Modulation & Stochastic p modes	Degroote et al. (2010)
HD 46202	8.19	O9V(f)	CoRoT	34.3	25	Heat-driven p modes	Briquet et al. (2011)
HD 44597	9.05	O9V	K2	33.1	~ 30	IGW?	this work
HD 256035	9.21	O9V:p+?	K2	33.1	270	Heat-driven modes	this work
HD 255055	9.40	O9V:p(e)	K2	33.1	~ 40	IGW?	this work
HD 149757	2.56	O9.5V _{nn}	WIRE,MOST,SMEI	232	400	Heat-driven p modes	Howarth et al. (2014)
EPIC 202060097	13.7	O9.5V	K2	33.1	?	Rotational Modulation	this work

binary HD 47129 is the only object in the list known to host a magnetic field and it is variable. Nevertheless, rotational modulation connected with chemical and/or temperature spots occurs for 4 of the 14 stars and is usually due to some level of magnetic activity even though the fields may be too weak or too complex to give detectable longitudinal field components.

From the viewpoint of seismic modelling with the aim to improve the input physics of massive star models, one needs to secure high-precision frequency values of several pulsation modes. While this is not impossible and has been achieved for a rapidly-rotating pulsating Be star (e.g. Neiner et al. 2012), it turned out hard to achieve so far in the case of internal gravity waves driven by the convective core in O stars (e.g. Aerts & Rogers 2015). The

requirement to detect oscillation frequencies with high precision of $\sim 0.0001 \text{ d}^{-1}$ can best be achieved in the case of self-driven modes caused by an opacity mechanism active in the partial ionisation layers of the iron-group elements, because they have long lifetime. HD 46202 is the only O-type star that has been modelled seismically so far (Briquet et al. 2011). While this led to the derivation of its fundamental parameters with higher precision than any other method delivered so far, it was not possible to probe its interior structure properties at a level necessary to improve the input physics of the models, due to the too short time base of the space data.

Heat-driven O-type pulsators hold the same potential of deep seismic sounding of their interior structure than was re-

cently achieved by Moravveji et al. (2015) for the B8.3V star KIC 10526294. This $3.2 M_{\odot}$ star provided seismic evidence for diffusive mixing in the stellar envelope at a level of $\log D_{\text{mix}}$ between 1.75 and 2.00 dex, in addition to core overshooting. A major improvement for evolutionary models of massive stars requires the observational calibration of the overall mixing properties in their interior, because theoretical considerations lead to $\log D_{\text{mix}}$ values differing by many orders of magnitude and are therefore of limited value for the moment (e.g., Mathis, Palacios, & Zahn 2004). Asteroseismology of O star pulsators is the best method to make progress for the tuning of models of the most massive stars in the Universe, but it requires long-term high-precision time-resolved photometric and spectroscopic monitoring. As we have shown in this work, the K2 mission has a major role to play here and EPIC 202060092 was an optimal target among five measured ones, but its complex beating pattern was not sufficiently sampled in terms of cadence, precision, and duration of the photometry achieved during Campaign 0. Moreover, it turned out to be a spectroscopic binary and we need to understand the contributions of each of its components to the detected variability. Requirements for its future seismic modelling are the accurate determination of its orbital properties and of the fundamental parameters of its binary components, along with a higher precision of the pulsation frequencies. Given its potential, spectroscopic monitoring will be continued in the coming years with the aim to unravel the orbital motion and to attempt detection of its oscillation modes in long-term residual spectroscopy.

Following Degroote et al. (2010) and Briquet et al. (2011), our current work is a successful proof-of-concept study to perform future O-star seismology. *This is possible with the optimised K2 mission in combination with ground-based spectroscopy.* Indeed, as of K2's Campaign 3, the improvement on its performance in terms of pointing and precision of the photometry, as well as in the duration of the campaigns (~ 80 d, i.e., twice to three times as long as the current study) holds the potential to deliver the appropriate photometric data needed for in-depth modelling of O-star pulsations, whatever their excitation mechanism. A light curve at short cadence during 80 d will deliver some 115 000 data points, which will result in a factor ~ 20 better frequency precision than for the Campaign 0 data. Given their scarcity and importance for stellar and galactic structure, we thus plan to apply for short-cadence data for the few available O stars in K2's future FoVs of Campaigns 11 and 13.

ACKNOWLEDGMENTS

Part of the research included in this manuscript was based on funding from the Research Council of KU Leuven, Belgium under grant GOA/2013/012, from the European Community's Seventh Framework Programme FP7-SPACE-2011-1, project number 312844 (SpaceInn), and from the Fund for Scientific Research of Flanders (FWO) under grant agreement G.0B69.13. Funding for the Kepler mission is provided by the NASA Science Mission directorate. The authors wish to thank the entire *Kepler* team and the *Kepler* Guest Observer Office for all their efforts.

REFERENCES

- Aerts C., 2015, IAUS, 307, 154
Aerts C., Rogers, T., 2015, ApJL, in press (arXiv1505.06648)
Aerts C., Puls J., Godart M., Dupret M.-A., 2009, A&A, 508, 409
Aerts, C., Christensen-Dalsgaard, J., & Kurtz, D. W. 2010, Asteroseismology, Springer, Heidelberg
Auvergne M., et al., 2009, A&A, 506, 411
Beck P. G., et al., 2014, A&A, 564, A36
Bedding T. R., et al., 2011, Natur, 471, 608
Bischoff-Kim A., Østensen R. H., 2011, ApJ, 742, L16
Blomme R., et al., 2011, A&A, 533, A4
Briquet M., et al., 2011, A&A, 527, A112
Chaplin W. J., Miglio A., 2013, ARA&A, 51, 353
Charpinet S., et al., 2011, A&A, 530, A3
Córscico A. H., Althaus L. G., Kepler S. O., Costa J. E. S., Miller Bertolami M. M., 2008, A&A, 478, 869
Cuypers J., et al., 2009, A&A, 499, 967
De Cat P., et al., 2007, A&A, 463, 243
Degroote P., et al., 2009, A&A, 506, 111
Degroote P., et al., 2010, A&A, 519, A38
Fullerton A. W., Gies D. R., Bolton C. T., 1996, ApJS, 103, 475
Grunhut J. H., et al., 2013, MNRAS, 428, 1686
Handler G., et al., 2004, MNRAS, 347, 454
Handler G., et al., 2006, MNRAS, 365, 327
Hermes J. J., et al., 2011, ApJ, 741, L16
Howarth I. D., Stevens I. R., 2014, MNRAS, 445, 2878
Howarth I. D., Goss K. J. F., Stevens I. R., Chaplin W. J., Elsworth Y., 2014, MNRAS, 440, 1674
Howell S. B., et al., 2014, PASP, 126, 398
Kurtz D. W., Saio H., Takata M., Shibahashi H., Murphy S. J., Sekii T., 2014, MNRAS, 444, 102
Lanz, T., & Hubeny, I. 2003, ApJS, 146, 417
Lehmann H., et al., 2011, A&A, 526, A124
Linder N., Rauw G., Martins F., Sana H., De Becker M., Gosset E., 2008, A&A, 489, 713
Loumos G. L., Deeming T. J., 1978, Ap&SS, 56, 285
Maeder A., 2009, Physics, Formation and Evolution of Rotating Stars, Springer, Heidelberg
Mahy L., et al., 2011, A&A, 525, A101
Mathis S., Palacios A., Zahn J.-P., 2004, A&A, 425, 243
Mathis S., Neiner C., Tran Minh N., 2014, A&A, 565, A47
Montgomery M. H., O'Donoghue D., 1999, DSSN, 13, 28
Mosser B., et al., 2012, A&A, 540, A143
Moravveji, E., et al. 2015, A&A, in press (arXiv:1505.06902)
Neiner, C., Floquet, M., Samadi, R., et al. 2012, A&A, 546, A47
Niemczura E., et al., 2015, MNRAS, 450, 2764
Østensen R. H., Bloemen S., Vučković M., Aerts C., Oreiro R., Kinemuchi K., Still M., Koester D., 2011, ApJ, 736, L39
Østensen R. H., et al., 2012, ApJ, 753, L17
Pápics P. I., et al., 2012, A&A, 542, A55
Pápics P. I., et al., 2013, A&A, 553, A127
Pápics P. I., Moravveji E., Aerts C., Tkachenko A., Triana S. A., Bloemen S., Southworth J., 2014, A&A, 570, A8
Pápics P. I., Tkachenko A., Aerts C., Van Reeth T., De Smedt K., Hillen M., Østensen R., Moravveji E., 2015, ApJ, 803, L25
Ramiaramanantsoa T., et al., 2014, MNRAS, 441, 910
Raskin G., et al., 2011, A&A, 526, A69
Rauw G., et al., 2008, A&A, 487, 659
Rogers T. M., Lin D. N. C., McElwaine J. N., Lau H. H. B., 2013, ApJ, 772, 21
Saesen S., Briquet M., Aerts C., Miglio A., Carrier F., 2013, AJ, 146, 102
Saio H., Kurtz D. W., Takata M., Shibahashi H., Murphy S. J., Sekii T., Bedding T. R., 2015, MNRAS, 447, 3264
Sana H., et al., 2012, Sci, 337, 444
Schwarzenberg-Czerny A., 2003, ASPC, 292, 383

- Tkachenko A., Lehmann H., Smalley B., Deboscher J., Aerts C.,
2012, MNRAS, 422, 2960
Tkachenko A., et al., 2013, A&A, 556, A52
Tkachenko A., et al., 2014, MNRAS, 442, 616
Vanderburg A., 2014, arXiv:1412.1827
Vanderburg A., Johnson J. A., 2014, PASP, 126, 948
Van Grootel V., et al., 2010, ApJ, 718, L97
Van Reeth T., et al., 2015, ApJS, in press (arXiv:1504.02119)
Van Winckel H., et al., 2009, A&A, 505, 1221

**APPENDIX A: MASKS FOR LIGHT CURVE
EXTRACTION**

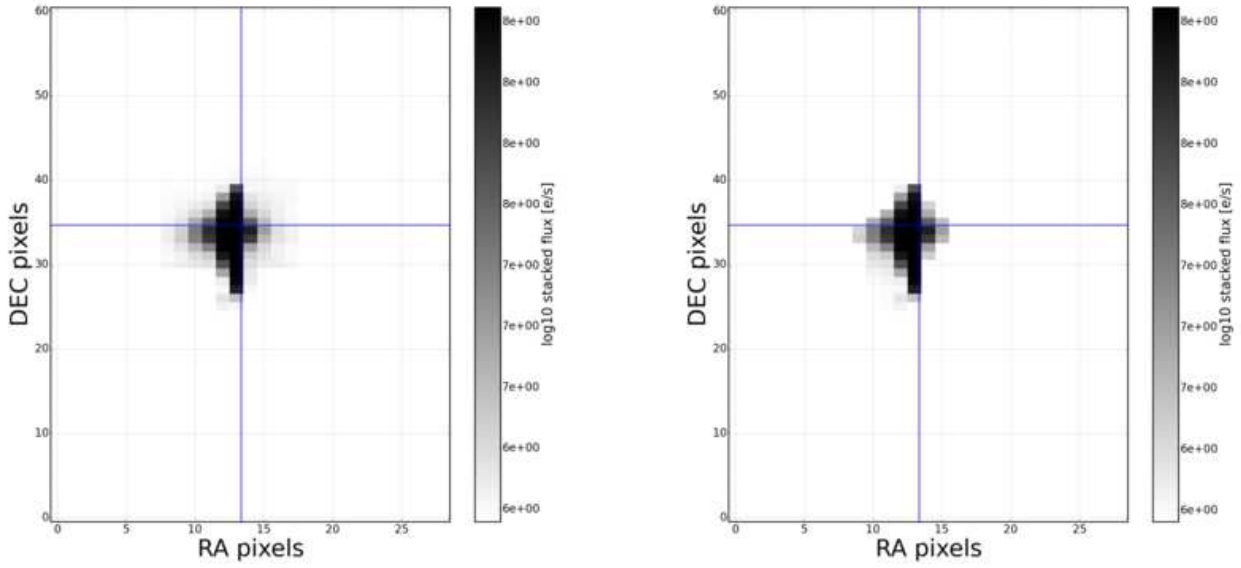


Figure A1. Our adopted mask (left) versus the one used by Vanderburg (right) for the light curve extraction of EPIC 202060091 as indicated in pink. The position of the star is indicated by the blue cross.

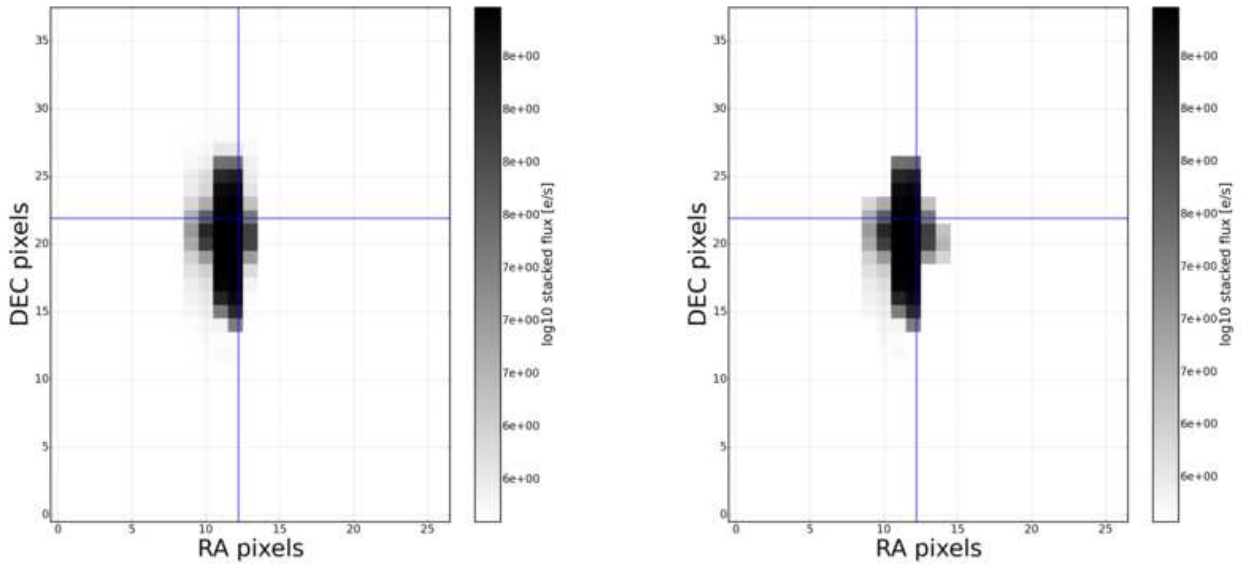


Figure A2. Same as Fig. A1, but for EPIC 202060092.

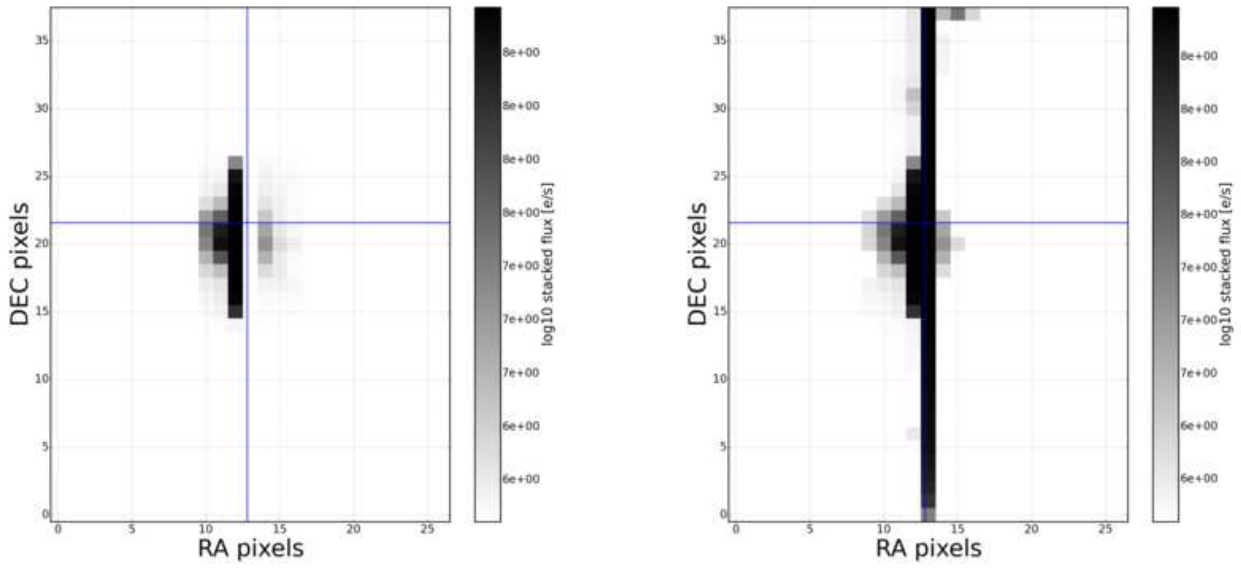


Figure A3. Same as Fig. A1, but for EPIC 202060093. For this target, the mask on the left excluded the central saturated column to produce the photometry shown as black circles in the top panel of Fig. 1, while this column was used to produce the Vanderburg version of the light curve shown as grey crosses in the top panel of Fig. 1.

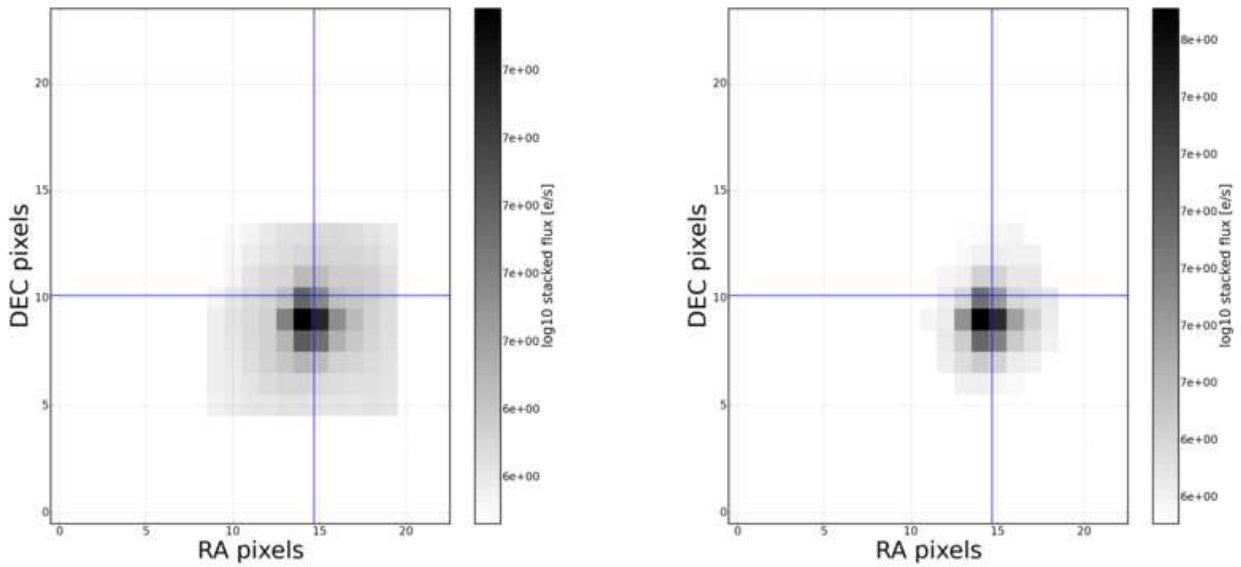


Figure A4. Same as Fig. A1, but for EPIC 202060097.

